Proceedings of the 5th WSEAS International Conference on Applied Computer Science, Hangzhou, China, April 16-18, 2006 (pp584-589)

CFD Simulations of Swirling Effects on the Performance of the Supersonic Nozzle for Micro-particle Delivery

Y. LIU*, G. COSTIGAN
Department of Engineering Science
University of Oxford
Oxford OX2 0EP, UNITED KINGDOM
Http: //www.eng.ox.ac.uk/pjrc

Abstract: A high-speed gas flow, generated by a miniature supersonic nozzle for microparticle acceleration, is investigated. In medical application, the powder formulation of drugs can be delivered into human skin or mucosal tissue for the treatment of a range of diseases. One of the main concerns for designing and evaluating such system is ensuing that microparticles are delivered into human skin with a controllable velocity range and spatial distribution. The initial experimental work suggested that the performance of the device strongly depends on the aerodynamics of the supersonic nozzles employed. In this paper, computational fluid dynamics is utilized to simulate a prototype device, with the aim of investigating the swirling flow in its supersonic nozzle. Swirling effects on the gas dynamics, vortex-shock interaction and performance are discussed.

Key-Words: - Nozzle, Numerical, Particle delivery, Simulation, Supersonic, Swirl

1 Introduction

We have proposed miniature rocket-like gene gun (PowderJect), which is created as a unique means of introducing powder drugs into human skin in response to the difficulty of getting macro-molecular agents across stratum corneum [1-5]. It harnesses energy of compressed helium gas to accelerate the micro-sized drugs through a supersonic nozzle up to a sufficient momentum to penetrate the outer layer of skin or mucosal tissue to directly target the cells of interest. There are many advantages over a conventional needle and syringe, in terms of effectiveness, cost and health risk.

Particle delivery efficiency and controllability are predominated by the quality of gas flow. Hence, it is imperative to optimise the nozzle design and its aerodynamics to achieve rapid and uniform mixing. The swirl is particularly suited to high-pressure ratio and high-area ratio operational condition of the PowderJect device, where intimate mixing of high-speed gas and particles is essential for the particle delivery system to achieve a more uniform spatial distribution and tight controlled velocity range [6-10]. The distribution of gas properties (*e.g.* velocity, density) needs to ensure not only maximum aerodynamic performance but also adequate penetration momentum for the particles. Preliminary studies have revealed that apart from enhancing the gas mixing, swirling also promotes the particle activity during the particle introduction from a cassette. It is particularly helpful for stick DNA-coated particles to be segregated to avoid potential skin damage. However, all these benefits are at the expense of an achievable particle penetration depth.

In this paper, we seek to employ computational fluid dynamics (CFD) to investigate the performance of a prototype PowderJect system. We begin with a brief description of the prototype device, followed by a presentation of the CFD methodology employed. The gas flow is modelled by solving a set of differential equations. The overall capability of delivering microparticles to human skin is analyzed through a series of numerical calculations. The primary emphasis of this study is to achieve new insights into swirling effects on the over-expanded supersonic nozzle flow.

2 Prototype Device and Geometry

Figure 1 shows an illustrative diagram of the prototype PowderJect device under the numerical concern.

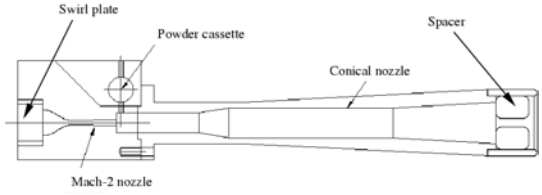

Figure 1. The prototype PowderJect device

Key components include a swirl plate, a Mach-2 nozzle, a conical nozzle consisting of two parallel and two diverging sections, powder cassette and spacer. The diameters of the Mach-2 nozzle throat and conical nozzle exit are 1.4 mm and 10 mm, respectively. Considering this area ratio and operating pressure of 2-6 MPa, the nozzle is working in over-expanded condition. Hence, the complicate shock interactions are expected.

Upon actuation, a compressed helium gas tangentially flows into swirl plate and aligns itself with the nozzle contours. Subsequently, a supersonic streamwise vortex is generated through the Mach-2 nozzle. This vortex then interacts with the shock system inherently in the conical nozzle when operated in a large pressure ratio. The interaction between a supersonic streamwise vortex and a shock wave is a natural extension of the incompressible vortex breakdown problem. It can significantly affect the aerodynamic performance characteristics of the PowderJect device.

Current designs of swirl components depend on extensively experimentation to arrive at satisfactory results in terms of delivery efficiency and penetration depth. Such experiments are expensive and time consuming given the vast number of parameter variations involved. A relatively small space (*e.g.* the diameter of the Mach-2 nozzle throat, 1.4 mm) and short period of operation time (< 3-5 ms) available for experimental implementation add further difficulties. On the other hand, advanced CFD simulation codes lend us an efficient and accurately tool of modelling such supersonic swirl flows. Therefore it is highly desirable to develop appropriate models to be incorporated in CFD codes that could be used to guide the optimisation of supersonic nozzle design [3-5]. In this paper, CFD is utilised to simulate swirling feature of the prototype PowderJect device, including formation of shock, vortex mixing, shock/boundary layer and shock/vortex interactions.

3 Computational Model

Considering the swirl plate, with geometric changes and flow gradients in the circumferential direction, a three-dimensional model is required. However, the predominant feature of the flow in the downstream Mach-2 and conical nozzles is axisymmetric with respect to geometry and flow conditions (illustrated in the simulation results later).

In order to quickly determine effects of various modeling and design choices, simplification of the problem of three-dimensional swirling flows to an equivalent two-dimensional axisymmetric problem can be very beneficial. Computational cost is very attractive, too. In this case, the flow is modeled by the axisymmetric equations, with prediction of the swirl velocity. Key point is that the assumption of axisymmetry indicates that there are no circumferential gradients, but swirl velocities.

3.1 Govenning Equations

The three-dimensional complete fluid equations and two-dimensional axisymmetric equations (with swirl) are given, respectively.

3.1.1 The mass conservation equations

The equation for conservation of mass, or continuity equation, can be written in the general form

$$\frac{\partial \rho}{\partial t} + \nabla \bullet (\rho \vec{v}) = S_m \qquad (1)$$

where ρ, t and $\vec{v}$ are the density, time and velocity vector, respectively; S_m is the mass source.

For two-dimensional axisymmetric geometries, the continuity equation is given by

$$\frac{\partial \rho}{\partial t} + \frac{1}{r}\frac{\partial}{\partial x}(r\rho v_x) + \frac{1}{r}\frac{\partial}{\partial r}(r\rho v_r) = S_m \qquad (2)$$

where x and r respectively denote the axial, radial coordinates; v_x and v_r are the axial, radial velocities.

3.1.2 The momentum conservation equations

Conservation of momentum is described as

$$\frac{\partial}{\partial t}(\rho \vec{v}) + \nabla \bullet (\rho \vec{v}\vec{v}) = -\nabla p + \nabla \bullet (\bar{\bar{\tau}}) + \rho \vec{g} + \vec{S}_F \qquad (3)$$

where p is the static pressure, $\bar{\bar{\tau}}$ is the stress tensor (described below), $\rho \vec{g}$ and $\vec{S}_F$ are the gravitational body force and external body forces, respectively.

The stress tensor $\bar{\bar{\tau}}$ is given by

$$\bar{\bar{\tau}} = \mu\left[(\nabla \vec{v} + \nabla \vec{v}^T) - \frac{2}{3}\nabla \bullet \vec{v} I\right]$$

where μ is the molecular viscosity, I is the unit tensor, and the second term on the right hand side is the effect of volume dilation.

For 2D axisymmetric geometries, the axial and radial momentum conservation equations are

$$\begin{aligned} &\frac{\partial}{\partial t}(\rho v_x) + \frac{1}{r}\frac{\partial}{\partial x}(r\rho v_x v_x) + \frac{1}{r}\frac{\partial}{\partial r}(r\rho v_r v_x) = -\frac{\partial p}{\partial x} \\ &\quad + \frac{1}{r}\frac{\partial}{\partial x}\left[r\mu\left(2\frac{\partial v_x}{\partial x} - \frac{2}{3}(\nabla \bullet \vec{v})\right)\right] \\ &\quad + \frac{1}{r}\frac{\partial}{\partial r}\left[r\mu\left(\frac{\partial v_x}{\partial r} + \frac{\partial v_r}{\partial x}\right)\right] + S_{Fx} \end{aligned} \qquad (4a)$$

$$\frac{\partial}{\partial t}(\rho v_r)+\frac{1}{r}\frac{\partial}{\partial x}(r\rho v_x v_r)+\frac{1}{r}\frac{\partial}{\partial r}(r\rho v_r v_r)=-\frac{\partial p}{\partial r}+\frac{1}{r}\frac{\partial}{\partial x}\left[r\mu\left(\frac{\partial v_x}{\partial r}+\frac{\partial v_r}{\partial x}\right)\right]+\frac{1}{r}\frac{\partial}{\partial r}\left[r\mu\left(2\frac{\partial v_r}{\partial r}-\frac{2}{3}(\nabla\bullet\vec{v})\right)\right]+S_{Fr}-2\mu\frac{v_r}{r^2}+\frac{2}{3}\frac{\mu}{r}(\nabla\bullet\vec{v})+\rho\frac{v_z^2}{r} \quad (4b)$$

where $\nabla\bullet\vec{v}=\frac{\partial v_x}{\partial x}+\frac{\partial v_r}{\partial r}+\frac{v_r}{r}$, v_z is the swirl velocity.

In the axisymmetric flows with swirl, the tangential momentum equation may read

$$\frac{\partial}{\partial t}(\rho v_z)+\frac{1}{r}\frac{\partial}{\partial x}(r\rho v_x v_z)+\frac{1}{r}\frac{\partial}{\partial r}(r\rho v_r v_z)=\frac{1}{r}\frac{\partial}{\partial x}\left[r\mu\frac{\partial v_z}{\partial x}\right]+\frac{1}{r^2}\frac{\partial}{\partial r}\left[r^3\mu\frac{\partial}{\partial r}\left(\frac{v_z}{r}\right)\right]-\rho\frac{v_r v_z}{r} \quad (4c)$$

3.1.3 The energy conservation equations

The equation for conservation of energy, is written in the general form

$$\frac{\partial}{\partial t}(\rho E)+\nabla\bullet\left(\vec{v}(\rho E+p)\right)=\nabla\bullet\left(k_{eff}\nabla T-\sum_j h_j J_j+(\vec{\tau}_{eff}\bullet\vec{v})\right)+S_h \quad (5)$$

where k_{eff} is the effective conductivity ($k_{eff}=k+k_t$, in which k_t is the turbulent thermal conductivity, defined according to the turbulence model), and J_j is the diffusion flux of species j. The first three terms on the right-hand side of Equation (5) represent energy transfer due to conduction, species diffusion, and viscous dissipation, respectively. S_h includes any other volumetric heat resources.

The 2D axisymmetric energy equation is

$$\frac{\partial}{\partial t}(\rho E)+\frac{1}{r}\frac{\partial}{\partial x}\left(r(\rho E+p)v_x\right)+\frac{1}{r}\frac{\partial}{\partial r}\left(r(\rho E+p)v_r\right)=+\frac{1}{r}\frac{\partial}{\partial x}\left[r\left(k_{eff}\nabla T-\sum_j h_j J_j+(\vec{\tau}_{eff}\bullet\vec{v})\right)v_x\right]+\frac{1}{r}\frac{\partial}{\partial r}\left[r\left(k_{eff}\nabla T-\sum_j h_j J_j+(\vec{\tau}_{eff}\bullet\vec{v})\right)v_r\right]+S_h \quad (6)$$

3.2 Turbulence Model

To appropriately model turbulent flow with a significant amount of swirl (*e.g.*, cyclone flows, swirling jets), the RNG-model is considered [11].

The RNG ***k-ε*** model is derived from the exact Navier-stokes equations, using a mathematical technique called Renormalization Group (RNG). The transport equation for **ε** differs from the standard ***k-ε*** model by new analytically determined constants and a new term

$$\frac{\partial}{\partial t}(\rho\varepsilon)+\frac{\partial}{\partial x_i}(\rho\varepsilon v_i)=\frac{\partial}{\partial x_j}(\alpha_\varepsilon\mu_{eff}\frac{\partial\varepsilon}{\partial x_j})+C_{1\varepsilon}\frac{\varepsilon}{k}G_k-C_{2\varepsilon}\rho\frac{\varepsilon^2}{k}-R_\varepsilon+S_\varepsilon$$

with $R_\varepsilon=\frac{C_\mu\rho\eta^3(1-\eta/\eta_0)}{1+\beta\eta^3}\frac{\varepsilon^2}{k}$, $\eta=Sk/\varepsilon$, $\eta_0=4.38$, $\beta=0.012$

where G_k, Y_M,(in ***k*** equation) and **S** are respectively the production of turbulence kinetic energy due to the mean velocity gradients [12], the contribution of dilatation-dissipation in compressible turbulence, and the modulus of the mean strain tensor. As a result, for weakly strained flow ($\eta\approx\eta_0$), R_ε term has no contribution, and RNG tends to give comparable results than the standard ***k-ε*** model. But in regions of large strain rate ($\eta>\eta_0$), this additional term may have a significant contribution, which yields a lower turbulent viscosity than the standard ***k-ε*** model. In addition, the inverse effective Prandtl numbers are computed using analytical formula derived by the RNG theory. In the same way, the model constants are also derived analytically: $C_{1\varepsilon}$=1.42, $C_{2\varepsilon}$=1.68. The eddy viscosity is calculated with the classical relation (C_μ=0.0845).

$$\mu_t=\rho C_\mu\frac{k^2}{\varepsilon}$$

For swirling flows encountered in the PowderJect devices, near-wall turbulence modeling is quite often a secondary issue. The fidelity of the predictions in these cases is mainly determined by the accuracy of the turbulence model in the core region. However, to minimize the sensitivity of pressure gradients, non-equilibrium wall function is used to improve the predictions, in addition to the special grid treatment near the nozzle wall.

3.3 Numerical Solver

The multi-species gas flow (the mixture of air and helium) is modeled, with a commercial CFD package FLUENT [13], by solving the governing equations (1, 3 and 5 for three-dimensional problem, 2, 4 and 6 for two-dimensional axisymmetric case), together with RNG ***k-ε*** model. For all equations, convective terms are discretized using a second-order upwind Roe's flux difference splitter scheme [14], achieving the necessary upwinding and dissipation close to shocks. The interface flux is determined by separate terms, which depends on the upstream and downstream sides of the face, so that the information passed through the face contains the flow characteristics. Diffusion terms are cast into a central difference form. The discretized algebraic equations are solved in a coupled way. The time marching procedure uses a first-order implicit Euler scheme. Other scalar equations (turbulence and species transport) are solved in a segregated manner.

3.4 Computational Grid

In Figure 2, the complete computational domain for the prototype device is illustrated, with the locations of boundary conditions specified.

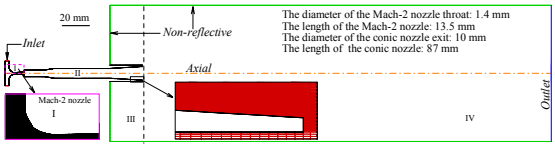

(a)

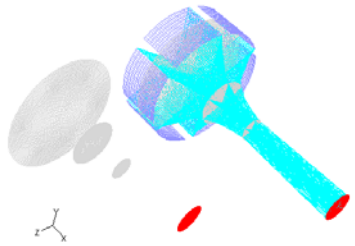

(b)

Figure 2. Illustrative diagram of computational domain and boundary conditions

The domain for two-dimensional axisymmetric simulations (Figure 2a) is extended to 30D×10D (D, diameter of the conical nozzle exit), to adapt the non-reflective and outlet boundary conditions (on the far-field boundaries). The grid has 30175 cells with 425 points along the axial direction and 71 points in the radial direction inside the Mach-2 and conic nozzles (Regions I and II, labeled in the figure). The mesh is bi-concentrated near the axis in order to capture vortex and mixing future, and the wall for a better boundary layer resolution with the first line cells at a distance of 15 μm away from the nozzle wall. Special care is given to the first cells, such that $y^+ \approx 6-50$, ($y^+ \equiv \rho u_\tau y / \mu$) at the wall-adjacent cells inside the conical nozzle. Finally, about 8000 cells are placed in Region IV and relaxed towards the outlet boundary, with the rest well distributed in Region III. In total, there are 39870 cells.

To make use of the periodic nature of the swirl plate (and the Mach-2 nozzle, too), one-sixth of volume is meshed and simulated for six-passage swirl plate (Figure 2b). The three-dimensional domain contains 23640 cells for the swirl plate, and 38800 for Mach-2 nozzle, respectively.

For the system shown in Figure 1, the flow released from the gas bottle to the swirl plate through an introduction passage is not simulated. Instead, the measured pressure is taken as the total pressure for the inlet flow. The wall temperature is assumed to be constant during operation (< 3-5 ms of interest for the particle delivery), with a non-slip condition. A non-reflective boundary condition is set for the far-field boundary. The atmospheric pressure is specified at the outlet boundary for subsonic flow in the two-dimensional axisymmetric case. In the three-dimensional swirl simulation, the outlet boundary condition is not needed due to a supersonic outflow.

CFD calculations with different combinations of grids, physical models and the particle drag correlations are conducted for the purpose of grid-independency study. The most important parameters have been monitored on different grids and differences no larger than 0.1% have been observed. Therefore, the influence of the discretization error is negligible for these numerical studies.

4 Results and Discussion

4.1 Axisymmetric Simulation without Swirl

As a baseline case, we initially simulated the flow for the total pressure of 4 MPa with no swirl specified in the inlet boundary. Figure 3 shows the calculated results, in terms of temperature, strain rate contours, and the velocity vectors of interest, illustrating the complexity of flow structures inside the prototype PowderJect device.

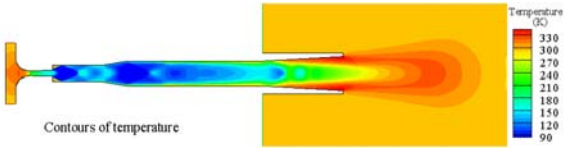

(a)

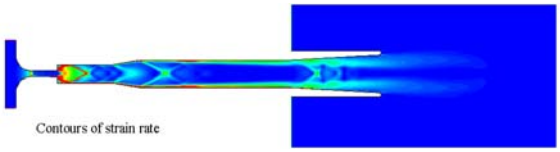

(b)

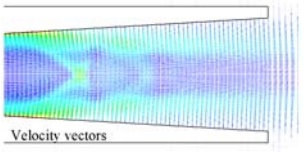

(c)

Figure 3. Simulated temperature (a), strain rate contours (b), and velocity vectors (c) of the axisymmetric flow

Figure 4 shows the streamlines in the nozzle without swirl, indicating a poor vortex mixing.

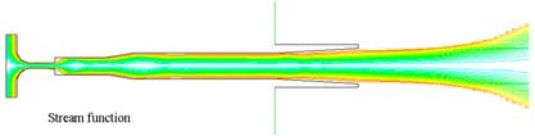

Figure 4. Simulated streamlines of the axisymmetric flow

4.2 Axisymmetric Simulation with Swirl

To interrogate swirl effects on the aerodynamic effect on the prototype device, we simulated axisymmetric swirl flows by including Eqn. 4c and imposing different swirl ratios at the inlet boundary. The swirl is measured by the swirl ratio, *i.e.*, the swirl velocity ($\mathbf{v_z}$) and the axis velocity ($\mathbf{v_x}$).

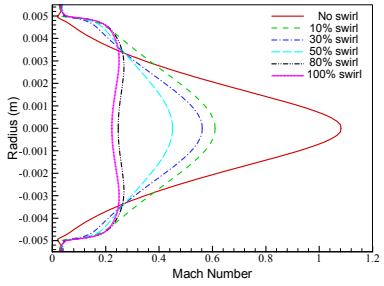

Figure 5. Mach number profiles at the conical nozzle exit with different inlet swirl ratios

Figure 5 plots the Mach number profiles at the nozzle exit with various swirl ratios. The moderately swirling helps the mixing, *i.e.*, to decrease core velocity peak (from supersonic to subsonic), and increase velocity near the nozzle edge. The relatively uniform distribution is achieved at 80% swirl ratio, with the exit Mach number of 0.24.

Alternatively, we extract the Mach number profiles along the central axis, shown in Figure 6, for three inlet swirl ratios. With a 100% swirl ratio, the vortex breakdown significantly decreases the downstream flow Mach number from the supersonic (1.15) to subsonic condition (0.24) at the nozzle exit.

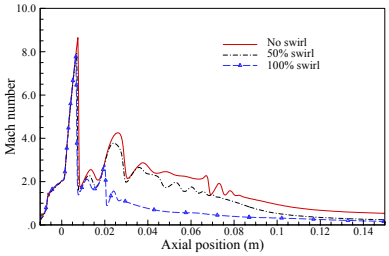

Figure 6. Mach number profiles along the central axis of the conical nozzle

Figure 7 traces the streamlines in the conical nozzle with 30% swirl ratio, showing the complexity of shock/vortex interaction inside the nozzle. Compared with the equivalence of no swirl case in Figure 4, we can clearly see the vortex breakdown pattern, with relatively large recirculation bubbles in the central area of beginning part of the second parallel section of the conical nozzle.

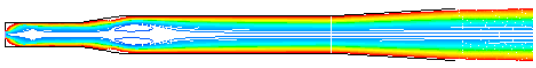

Figure 7. Flow streamlines with 30% inlet swirl ratio

4.3 Three-dimensional Simulation

The quoted swirl ratio is obtained by the design of an additional component, called swirl plate (Fig. 1), which is assembled upstream of the Mach-2 nozzle. The helium, released from gas-cylinder, is guided into the nozzle through a number of passages tangentially or radially. The generated swirl ratio depends on the numbers of passages and direction.

To examine the validity of the two-dimensional axisymmetric simulations, we simulated the combined configuration of a six-passage swirl plate and a Mach-2 nozzle. A one-sixth of volume is meshed and calculated due to the periodic geometry and flow condition.

Figure 8 shows typical results for three-dimensional simulation, with six passages even distributed along the surface.

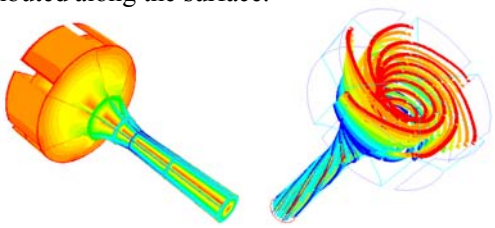

(a) Pressure contours and flow path

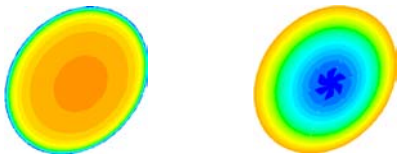

(b) Mach number and pressure contours at the nozzle exit with swirl (tangentially inlet)

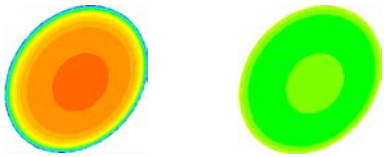

(c) Mach number and pressure contours at the nozzle exit without swirl (radially inlet)

Figure 8. Simulated three-dimensional results

One can see three-dimensional view of pressure contours in Figure 8a, together with flow path visualization, characterizing the vortex generation. The Mach number and pressure plane distributions at the nozzle exit are shown in Figure 8b. An almost axisymmetric flow pattern is obviously exhibited, except for the pressure contours where the six-passage inlets are resembled. Noted that this visible pressure non-axisymmetric feature is due to a narrow colour bar. As a comparison, in Figure 8c, we present the results for the same geometry and flow condition, but with radially flow inlet direction, referred as no swirl. An

axisymmetric feature is well preserved. It is demonstrated that the axisymmetric assumption is reasonable to mimic the three-dimensional flow characteristics.

Now we turn our attention to the particle dynamics, to investigate the swirl on the particle distribution and penetration depth. It is studied by experimental penetration. Figure 9 shows a typical particle `footprint' with no-swirl and two-passage swirl plate. With swirling, more particles are distributed towards outside of target area. This is consistent with the predicted gas flow field and particle simulations.

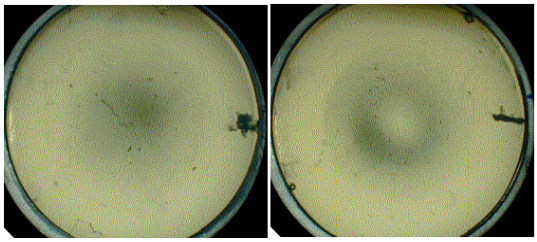

Figure 9. Sampled particle penetration footprints

5 Conclusion

Swirl effects on the gas and particle dynamics within a prototype PowderJect device have been investigated numerically. A CFD approach has been implemented in order to gain new insights into the behavior of swirl flow in the supersonic nozzle.

The calculations reveal that a large area ratio and operating pressure condition result in over-expanded nozzle operation. Without swirl, a non-uniform gas distribution is generated due to oblique shock systems inherently within the supersonic nozzle. CFD simulations demonstrate that the PowderJect device with a relative small swirl can enhance vortex mixing, achieving a much improved gas velocity range and spatial distribution, without decreasing the penetration momentum too much.

The numerical investigations also show that the axisymmetric assumption is valid in the present three-dimensional swirl effect studies with a great computational efficiency.

These calculations can provide us the guideline to optimize the delivery system, with particles delivered into the target with a desired swirl ratio.

References:

1. B.J. Bellhouse, D.F. Sarphie and J.C. Greenford, Needless Syringe Using Supersonic Gas Flow for Particle Delivery, Int. Patent WO94/24263, 1994.
2. G. Costigan, Y. Liu, G.L. Brown, F.V. Carter and B.J. Bellhouse, Evolution of the design of the venturi devices for the delivery of dry particles to skin or mucosal tissue, Paper-2981, Proc. of 24th Int. Symp. on Shock Waves, Beijing, PR China, 2004
3. Y. Liu, G. Costigan and B.J. Bellhouse, Aerodynamic performance of an earlier venturi powdered vaccines/drug delivery system, AIAA-2005-5005, 35th AIAA Fluid Dynamics Conference and Exhibit, Toronto, Canada, 2005
4. Y. Liu, M.A.F. Kendall, N.K. Truong and B.J. Bellhouse, Numerical and experimental analysis of a high speed needle-free powdered vaccines delivery device, AIAA-2002-2807, Proc. 20th AIAA Applied Aerodynamics Conference, St. Louis, MO, USA, 2002
5. Y. Liu and B.J. Bellhouse, Prediction of jet flows in the supersonic nozzle and diffuser, Int. J. for Numer. Meth. in Fluids, 47, pp:1147-1155, 2005
6. M.R. Ruith, P. Chen, E. Meiburg and T. Maxworthy, Three-dimensional vortex breakdown in swirling jets and wakes: direct numerical simulations, J. Fluid Mech., 486, pp:331-371, 2003
7. J.E. Martin and E. Meiburg, Nonlinear axisymmetric and three-dimensional vorticity dynamics in a swirling jet model, Phys. Fluids, 8(7), pp:1917-1928, 1996
8. L.N. Cattafesta, III and G.S. Settles, Experiments on shock/vortex interactions, AIAA-92-0315, 1992
9. A.J. Fitzgerald, K. Hourigan and M.C. Thompson, Towards a universal criterion for predicting vortex breakdown in swirling jets, Proc. of the 15th Australasian Fluid Mechanics Conference, 2004
10. G.L. Brown and J.M. Lopez, Axisymmetric vortex breakdown Part 2. Physical mechanisms. J. Fluid Mech. 221, pp:553-576, 1990
11. D. Choudhury, Introduction to the renormalization group method and turbulence modeling, Tech. Rep. TM-107, Fluent Inc., Lebanon, USA, 1993
12. B. Launder and D. Spalding, Lectures in mathematical models of turbulence, Academic Press, London, England, 1972
13. Fluent user's guide volume, Fluent Inc. Also see, http://www.fluent.com/.
14. P. Roe, Approximate rieman solvers, parameters vectors, and difference schemes, J. Comput. Phys. 43, pp:357–372, 1981